JOURNAL OF MULTIFUNCTIONAL MATERIALS & PHOTOSCIENCE
11(2), December 2020, pp. 139-147

Synthesis of Microcrystalline $AgGd(MoO_4)_2$:Yb^{3+}/Ho^{3+}/Tm^{3+} Upconversion Phosphors and Their Spectroscopic Properties

Won-Chun Oh, Zambaga Otgonbayar, Md Nazmodduha Rafat, Kamrun Nahar Fatema, Chang Sung Lim*

Department of Aerospace Advanced Materials & Chemical Engineering, Hanseo University, Seosan 31962, Republic of Korea
Corresponding author: cslim@hanseo.ac.kr

Abstract: Microwave employed sol-gel (MES) derived Ho^{3+}/Yb^{3+}/Tm^{3+} tri-doped $AgGd_{1-x}(MoO_4)_2$ white phosphors were successfully synthesized with variations of Ho^{3+}, Yb^{3+} and Tm^{3+} (x = Ho^{3+} + Yb^{3+} + Tm^{3+}, Ho^{3+} = 0.04, 0.03, 0.02, 0.01, Yb^{3+} = 0.35, 0.40, 0.45, 0.50 and Tm^{3+} = 0.01, 0.02, 0.03, 0.04), and the crystal structure, concentration effect and spectroscopic characteristics were investigated. X-ray diffraction (XRD) and scanning electron microscopy (SEM) were employed to evaluate the crystalline structure and morphology All XRD peaks were identified by tetragonal cell ($I4_1/a$) with parameters close to $AgEu(MoO_4)_2$ and $NaGd(MoO_4)_2$. The site of (Ag/Eu) or (Na/Gd) ion was occupied by Ag, Gd, Ho, Yb, Tm ions with fixed occupations. The synthesized particles have been fairly crystallized and showed a homogeneous microcrystalline morphology with particle sizes of 3-5 ¼m. The spectroscopic properties were examined comparatively using upconversion photoluminescence emission, Commission Internationale de L'Eclairage (CIE) chromatic coordinates and Raman spectroscopy.

Keywords: Microwave sol-gel, Double molybdate, White phosphors, Upconversion, Spectroscopic Properties

1. Introduction

Recently, rare-earth (RE) doped upconversion (UC) phosphors extensively explored to the highly evaluated characteristics under special output emissions and finely crystallized structures in the field of optoelectronics such as for solid state laser devices, display technology, Light emitting diode (LED) materials, solar energy cell compositions, and biological imaging sensors [1-3]. Among such crystals, scheelite-type (ST) molybdates are widely investigated in terms of searching new structures, including structure-modulation effects [4-6], promising spectroscopic characteristics and excellent UC photoluminescence (PL) properties [7,8].

RE-doped molybdate materials have the tetragonal structure, space group $I4_1/a$, and belong to the family of ST structures. The trivalent RE ions, such as Ho^{3+}, Tm^{3+}, Er^{3+}

as an activator and Yb^{3+} as a sensitizer, can be partially and easily substituted in the host tetragonal stable crystalline phase [9-11]. During UC process, the ions of Ho^{3+} and Tm^{3+} have very effective energy band and suitable level configuration to convert from infrared to visible light. As a sensitizer, the Yb^{3+} ion can be smoothly excited by proper incident low energy light source. The tri-doped Yb^{3+}, Ho^{3+} and Tm^{3+} ions can remarkably enhance the UC efficiency for the shift from infrared to visible light due to the efficiency of the energy transfer from Yb^{3+} to Ho^{3+} and Yb^{3+} to Tm^{3+}. Ho^{3+} exhibits $^5S_2$/ $^5F_4$ '! $^5I_8$ transitions in the green region, $^5F_5$ '! $^5I_8$ transitions in the red region in UC process, while Tm^{3+} shows the $^1G_4$ '! $^3H_6$ transitions in the blue region, and $^1G_4$ '! $^3F_4$ and $^3H_4$ '! $^3H_6$ transitions in the red region, resulted by the consequent energy-transfer (ET) from Yb^{3+} to Ho^{3+} and Yb^{3+} to Tm^{3+} [12-14]. According to the present synthesized methods for UC compounds, microwave employed sol-gel (MES) process has its advantages of a very short process time, stable and homogenous particles, suitable particle size for UC process, and highly purified resultant product [15-20]. However, the crystal structure of the Ag, Gd containing double molybdates of $AgLn(MoO_4)_2$ (Ln = La, Gd, Y) are less clear, and UC properties using tri-doped Yb^{3+}, Ho^{3+} and Tm^{3+} ions in $AgGd_{1-x}(MoO_4)_2$ (AGM) and spectroscopic characteristics have not been reported.

In the present study, AGM:Ho^{3+}/Yb^{3+}/Tm^{3+} double molybdates under various concentration variations of Ho^{3+}, Yb^{3+} and Tm^{3+} (x = Ho^{3+} + Yb^{3+} + Tm^{3+}, Ho^{3+} = 0.04, 0.03, 0.02, 0.01, Yb^{3+} = 0.35, 0.40, 0.45, 0.50 and Tm^{3+} = 0.01, 0.02, 0.03, 0.04) were successfully prepared by the MES method, followed by heat treatment. X-ray diffraction (XRD) and scanning electron microscopy (SEM) were employed to evaluate the crystalline structure and morphology. The resultant phosphors were evaluated by the PL measurements accompanying the pump power dependence derived from the UC emissions. The Commission Internationale de L'Eclairage (CIE) chromatic coordinates were provided, and Raman spectroscopic properties were discused in detail.

2. Experimental

In the present experiment, the fabrication of $AgGd_{1-x}(MoO_4)_2$:Ho^{3+}/Yb^{3+}/Tm^{3+} (AGM:HoYbTm) double molybdates under various concentration variations of Ho^{3+}, Yb^{3+} and Tm^{3+} (x = Ho^{3+} + Yb^{3+} + Tm^{3+}, Ho^{3+} = 0.04, 0.03, 0.02, 0.01, Yb^{3+} = 0.35, 0.40, 0.45, 0.50 and Tm^{3+} = 0.01, 0.02, 0.03, 0.04) was aimed at the MES process. In the preparation of starting materials, $AgNO_3$ with purity 99.9% were received from Kojima Chemicals, Japan, $(NH_4)_6Mo_7O_{24}$'Š$4H_2O$ in purity of 99.0%, $Gd(NO_3)_3$'Š$6H_2O$, $Tm(NO_3)_3$'Š$5H_2O$, $Yb(NO_3)_3$'Š$5H_2O$ and $Ho(NO_3)_3$'Š$5H_2O$ in purity of 99.9% were used as received from Sigma-Aldrich, USA. Besides, citric acid (CA) in purity of 99.5% was received from Daejung Chemicals, Korea. Distilled water (DW), ethylene glycol (EG, A.R.) and NH_4OH (A.R.) were used to bring the transparent sol formation.

As the first sequence, to prepare the sol state of (a) AGM, $(NH_4)_6Mo_7O_{24}$'Š$4H_2O$ for 0.114 mol% was slowly dissolved in 80 mL of NH_4OH (8M) with 20 mL of EG under a slight heat-treatment. Simultaneously, $AgNO_3$ for 0.4 mol% and $Gd(NO_3)_3$'Š$5H_2O$ for 0.4 mol% were carefully weighed and dissolved very slowly in 100 mL of DW under a

slight heat treatment. Then, these two solutions were combined under a vigorous stirring. The CA molar ratio accounting to the numbers of all cation metal (CM) ions should be adjusted to 2:1 (CA/CM). The total volume of the combined solution, 180–200 mL, was heat-treated at ~80–100 °C in Pyrex glass (450 mL) before the MES processing. Finally, the consequent solution reveals a highly transparent state.

As for the doped compounds of $AgGd_{1-x}(MoO_4)_2$:Ho^{3+}/Yb^{3+}/Tm^{3+}, the following variations were made for which to prepare the solutions: (b) $AgGd_{0.60}(MoO_4)_2$:$Ho_{0.04}$/$Yb_{0.35}$/$Tm_{0.01,}$ 0.4 mol% $AgNO_3$ and 0.114 mol% $(NH_4)_6Mo_7O_{24}$'"$4H_2O$, 0.24 mol% $Gd(NO_3)_3$'"$6H_2O$ with 0.016 mol% $Ho(NO_3)_3$'"$5H_2O$, 0.14 mol% $Yb(NO_3)_3$'"$5H_2O$ and 0.004 mol% $Tm(NO_3)_3$'"$5H_2O$; (c) $AgGd_{0.55}(MoO_4)_2$:$Ho_{0.03}$/$Yb_{0.40}$/$Tm_{0.02,}$ 0.22 mol% $Gd(NO_3)_3$'"$6H_2O$, 0.012 mol% $Ho(NO_3)_3$'"$5H_2O$, 0.16 mol% $Yb(NO_3)_3$'"$5H_2O$ and 0.008 mol% $Tm(NO_3)_3$'"$5H_2O$; (d) $AgGd_{0.50}(WO_4)_2$:$Ho_{0.02}$/$Yb_{0.45}$/$Tm_{0.03,}$ 0.20 mol% $Gd(NO_3)_3$'"$6H_2O$, 0.008 mol% $Ho(NO_3)_3$'"$5H_2O$, 0.18 mol% $Yb(NO_3)_3$'"$5H_2O$ and 0.012 mol% $Tm(NO_3)_3$'"$5H_2O$; (e) $AgGd_{0.45}(WO_4)_2$:$Ho_{0.01}$/$Yb_{0.50}$/$Tm_{0.04,}$ 0.18 mol% $Gd(NO_3)_3$'"$6H_2O$, 0.004 mol% $Ho(NO_3)_3$'"$5H_2O$, 0.20 mol% $Yb(NO_3)_3$'"$5H_2O$ and 0.016 mol% $Tm(NO_3)_3$'"$5H_2O$. The MES derived process has been previously reported in the references [15-19].

The powder diffraction patterns of the AGM:HoYbTm particles were precisely examined over the range of 2è = 5-90° at room temperature with a D/MAX 2200 (Rigaku in Japan) diffractometer with Cu-Ká radiation and è-2è geometry. The typical microstructure and surface morphology of the obtained particles were observed using SEM (JSM-5600, JEOL in Japan). The PL spectra were relatively recorded using a spectrophotometer (Perkin Elmer LS55 in UK) at room temperature. Raman spectra measurements were performed using a LabRam Aramis (Horiba Jobin-Yvon in France) with the spectral resolution of 2 cm^{-1}. The 514.5-nm line of an Ar ion laser was used as an excitation source; the power on the samples was kept at the 0.5 mW level to avoid the sample decomposition.

3. Results and Discussion

Fig. 1 shows XRD patterns of the synthesized (a) $AgGd_{0.60}(MoO_4)_2$:$Ho_{0.04}$/$Yb_{0.35}$/$Tm_{0.01,}$ (b) $AgGd_{0.55}(MoO_4)_2$:$Ho_{0.03}$/$Yb_{0.40}$/$Tm_{0.02,}$ (c) $AgGd_{0.50}(MoO_4)_2$:$Ho_{0.02}$/$Yb_{0.45}$/$Tm_{0.03}$, and (d) $AgGd_{0.45}(MoO_4)_2$:$Ho_{0.01}$/$Yb_{0.50}$/$Tm_{0.04,}$ particles. All XRD peaks were identified by the previously reported AGM:HoYb system [20], which had been indexed by the tetragonal cell ($I4_1/a$) with parameters close to $AgEu(MoO_4)_2$ [21] and $NaGd(MoO_4)_2$ [22, 23]. Based on the Rietveld refinement of the AGM:HoYb system, the site of (Ag/Eu) or (Na/Gd) ion was occupied by Ag, Gd, Ho, Yb ions with fixed occupations according to suggested formulas, resulting stable and gives low R-factors [20]. The ST tetragonal phase of AGM:HoYbTm particles can be prepared by the MES method, followed post heat-treatment, to achieve a well-defined crystalline morphology. The compounds need to be heat treated at 850°C for 16 h. It is assumed that the doping amount of Ho^{3+}+Tm^{3+}/Yb^{3+} has a great effect on the crystalline cell volume of the AGM, because of the different ionic sizes. This means that the obtained samples possess a tetragonal-phase after partial substitution of Gd^{3+} by Ho^{3+}, Yb^{3+} and Tm^{3+} ions. The ions are effectively doped into crystal lattices of the AGM phase due to the substitution of Ho^{3+} (R=1.015 Å), Yb^{3+} (R=0.985 Å) and Tm^{3+} (R=0.994 Å) ions in the Gd^{3+} (R=1.053 Å) sites [24].

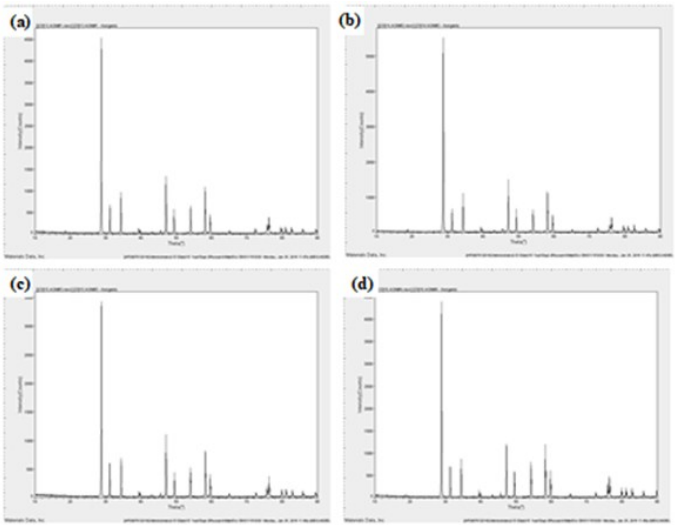

Fig. 1: XRD patterns of the synthesized (a) $AgGd_{0.60}(MoO_4)_2:Ho_{0.04}/Yb_{0.35}/Tm_{0.01,}$ (b) $AgGd_{0.55}(MoO_4)_2:Ho_{0.03}/Yb_{0.40}/Tm_{0.02,}$ (c) $AgGd_{0.50}(MoO_4)_2:Ho_{0.02}/Yb_{0.45}/Tm_{0.03}$, and (d) $AgGd_{0.45}(MoO_4)_2:Ho_{0.01}/Yb_{0.50}/Tm_{0.04,}$ particles.

Fig. 2 provides SEM images of the synthesized (a) $AgGd_{0.60}(MoO_4)_2:Ho_{0.04}/Yb_{0.35}/Tm_{0.01,}$ (b) $AgGd_{0.55}(MoO_4)_2:Ho_{0.03}/Yb_{0.40}/Tm_{0.02,}$ (c) $AgGd_{0.50}(MoO_4)_2:Ho_{0.02}/Yb_{0.45}/Tm_{0.03}$, and (d) $AgGd_{0.45}(MoO_4)_2:Ho_{0.01}/Yb_{0.50}/Tm_{0.04,}$ particles. It is seen that the as-synthesized samples reveal a fine and homogeneous morphology and the characteristic particle size is 3-5 ìm. The particles are partly coalesced into agglomerates and this is induced by inter-diffusions among the grains at 600-850°C. The samples have no discrepancy in aspect of morphological feature. It means that the morphological feature is insensitive to the $Ho^{3+}/Yb^{3+}/Tm^{3+}$ doping AGM lattice.

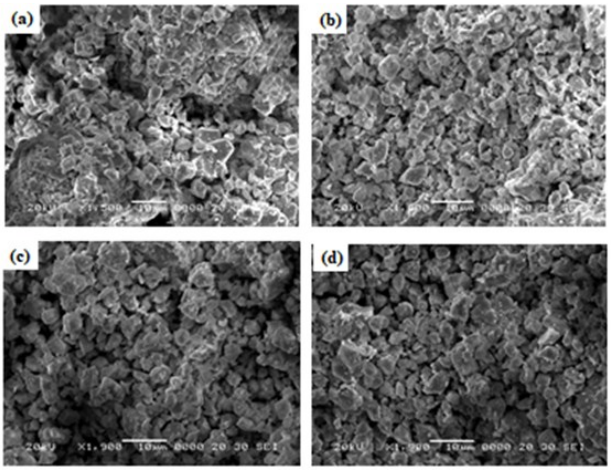

Fig. 2: SEM images of the synthesized (a) $AgGd_{0.60}(MoO_4)_2:Ho_{0.04}/Yb_{0.35}/Tm_{0.01,}$ (b) $AgGd_{0.55}(MoO_4)_2:Ho_{0.03}/Yb_{0.40}/Tm_{0.02,}$ (c) $AgGd_{0.50}(MoO_4)_2:Ho_{0.02}/Yb_{0.45}/Tm_{0.03}$, and (d) $AgGd_{0.45}(MoO_4)_2:Ho_{0.01}/Yb_{0.50}/Tm_{0.04,}$ particles.

Fig. 3 shows the UC output emission spectra of (a) $AgGd_{0.60}(MoO_4)_2$:$Ho_{0.04}$/$Yb_{0.35}$/$Tm_{0.01,}$ (b) $AgGd_{0.55}(MoO_4)_2$:$Ho_{0.03}$/$Yb_{0.40}$/$Tm_{0.02,}$ (c) $AgGd_{0.50}(MoO_4)_2$:$Ho_{0.02}$/$Yb_{0.45}$/$Tm_{0.03}$, and (d) $AgGd_{0.45}(MoO_4)_2$:$Ho_{0.01}$/$Yb_{0.50}$/$Tm_{0.04,}$ particles excited under 980 nm at room temperature. The doped particles exhibited white emissions corresponding to the $^1G_4$ '! $^3H_6$ transitions of Tm^{3+} in the blue region, the $^5S_2$/ $^5F_4$ '! $^5I_8$ transitions of Ho^{3+} in the green region, the $^5F_5$ '! $^5I_8$ transitions of Ho^{3+} as well as the $^1G_4$ '! $^3F_4$ and $^3H_4$ '! $^3H_6$ transitions of Tm^{3+} in the red region. The resultant UC intensity of (c) $AgGd_{0.50}(MoO_4)_2$:$Ho_{0.02}$/$Yb_{0.45}$/$Tm_{0.03}$ exhibits the proper intensities of the 475-nm, 545-nm and 655-nm emission band in the blue, green and red regions for white emissions, respectively. Otherwise, the UC intensity of (d) $AgGd_{0.45}(WO_4)_2$:$Ho_{0.01}$/$Yb_{0.50}$/$Tm_{0.04}$ reveals the strongest 545-nm emission band in the blue region and the strongest 655-nm emission band in the red region due to higher content of Tm^{3+}. Consequently, the optimal Yb^{3+}: Ho^{3+}+Tm^{3+} ratio is as high as 9:1 for white emitting diodes based on the proper blue, green and red emissions. The resultant UC particles revealed to the white output emissions and energy transfer such as an exchange interaction, which can promote non-radiative pole interactions [25].

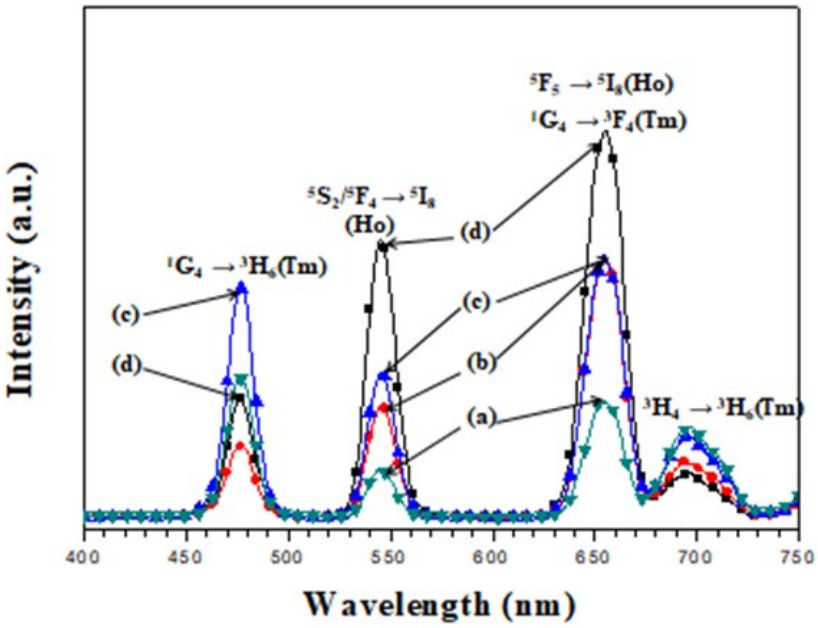

Fig. 3: UC PL emission spectra of (a) $AgGd_{0.60}(MoO_4)_2$:$Ho_{0.04}$/$Yb_{0.35}$/$Tm_{0.01,}$ (b) $AgGd_{0.55}(MoO_4)_2$:$Ho_{0.03}$/$Yb_{0.40}$/$Tm_{0.02,}$ (c) $AgGd_{0.50}(MoO_4)_2$:$Ho_{0.02}$/$Yb_{0.45}$/$Tm_{0.03}$, and (d) $AgGd_{0.45}(MoO_4)_2$:$Ho_{0.01}$/$Yb_{0.50}$/$Tm_{0.04,}$ particles excited under 980 nm at room temperature.

In Fig. 4, (A) the calculated chromaticity coordinates (x, y) and (B) CIE chromaticity diagram are shown for the compositions of UC output emission spectra of (a) $AgGd_{0.60}(MoO_4)_2$:$Ho_{0.04}$/$Yb_{0.35}$/$Tm_{0.01,}$ (b) $AgGd_{0.55}(MoO_4)_2$:$Ho_{0.03}$/$Yb_{0.40}$/$Tm_{0.02,}$ (c) $AgGd_{0.50}(MoO_4)_2$:$Ho_{0.02}$/$Yb_{0.45}$/$Tm_{0.03}$, and (d) $AgGd_{0.45}(MoO_4)_2$:$Ho_{0.01}$/$Yb_{0.50}$/$Tm_{0.04,}$ particles. The triangle depicted in Fig. 5(B) indicates standard coordinates for blue, green

and red colors. The inset in Fig. 5(B) shows the chromaticity points for the samples (a), (b), (c) and (d). As shown in Fig. 5(A), the calculated chromaticity coordinates x = 0.335 and y = 0.349 for (a) $AgGd_{0.60}(MoO_4)_2$:$Ho_{0.04}/Yb_{0.35}/Tm_{0.01}$, and x = 0.336 and y = 0.339 for (b) $AgGd_{0.55}(MoO_4)_2$:$Ho_{0.03}/Yb_{0.40}/Tm_{0.02,}$, x = 0.329 and y = 0.334 for (c) $AgGd_{0.50}(MoO_4)_2$:$Ho_{0.02}/Yb_{0.45}/Tm_{0.03}$, and x = 0.330 and y = 0.331 for (d) $AgGd_{0.45}(MoO_4)_2$:$Ho_{0.01}/Yb_{0.50}/Tm_{0.04}$ are corresponding to the standard equal energy point in CIE diagram in Fig.5(B).

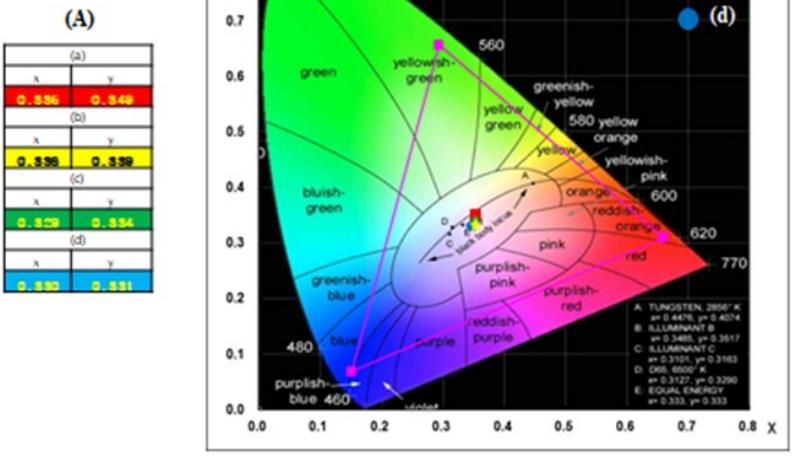

Fig. 4 : (A) Calculated chromaticity coordinates (x, y) values and (B) CIE chromaticity diagram for $NaGd_{1-x}(WO_4)_2$:$Ho^{3+}/Yb^{3+}/Tm^{3+}$ phosphors. The inset shows the emission points for the sample synthesized (a) $AgGd_{0.60}(MoO_4)_2$:$Ho_{0.04}/Yb_{0.35}/Tm_{0.01,}$ (b) $AgGd_{0.55}(MoO_4)_2$:$Ho_{0.03}/Yb_{0.40}/Tm_{0.02,}$ (c) $AgGd_{0.50}(MoO_4)_2$:$Ho_{0.02}/Yb_{0.45}/Tm_{0.03}$, and (d) $AgGd_{0.45}(MoO_4)_2$:$Ho_{0.01}/Yb_{0.50}/Tm_{0.04,}$ particles.

Fig. 5 shows the Raman spectra of the synthesized (a) pure AGM, (b) $AgGd_{0.60}(MoO_4)_2$:$Ho_{0.04}/Yb_{0.35}/Tm_{0.01,}$ (c) $AgGd_{0.55}(MoO_4)_2$:$Ho_{0.03}/Yb_{0.40}/Tm_{0.02,}$ (d) $AgGd_{0.50}(MoO_4)_2$:$Ho_{0.02}/Yb_{0.45}/Tm_{0.03}$, and (e) $AgGd_{0.45}(MoO_4)_2$:$Ho_{0.01}/Yb_{0.50}/Tm_{0.04,}$ particles. The internal modes for the (a) pure AGM particles were detected at 160, 200, 322, 388, 811, and 881 cm^{-1}, respectively. All compounds under consideration have the tetragonal ST-type structure (space group $I4_1/a$, C_{4h}^{6} symmetry) and they consist of MoO_4 tetrahedral and $(Ag/Gd/Ho/Yb/Tm)O_8$ polyhedral. The high-frequency boundary of spectral bands related to the vibrations of AGM structural units is expressed by a high-intensity peak of the ν_1 MoO_4 symmetric stretching vibration typical of ST molybdates [8, 15-20]. The Raman spectrum of the AGM crystal in Fig. 5(a) shows the typical molybdate compounds, which is divided into two parts with a wide empty gap of 400-750 cm^{-1} [26, 27]. The Raman spectra of the doped particles indicate the very strong and dominant peaks at higher frequencies of 811, 881, 1120 and 1283 cm^{-1} and at lower frequencies of 160, 204, 322 and 396 cm^{-1}.

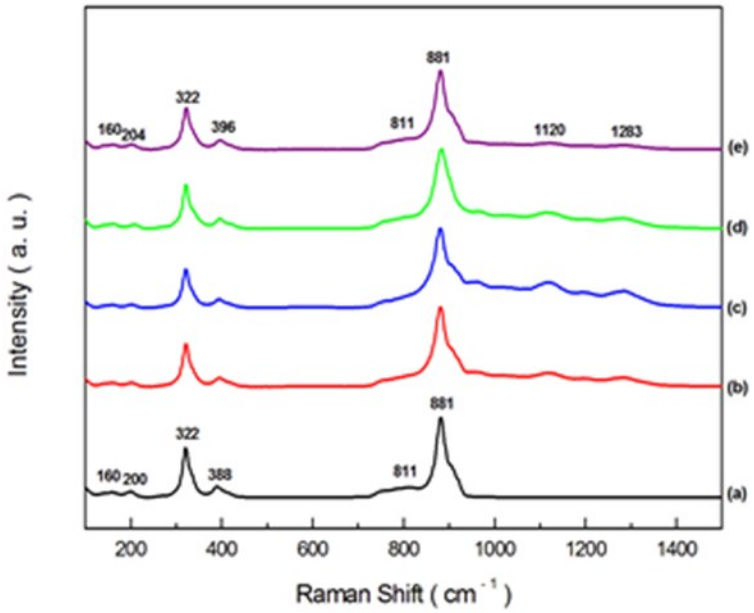

Fig. 5: Raman spectra of the synthesized (a) pure AGM, (b) $AgGd_{0.60}(MoO_4)_2:Ho_{0.04}/Yb_{0.35}/Tm_{0.01,}$ (c) $AgGd_{0.55}(MoO_4)_2:Ho_{0.03}/Yb_{0.40}/Tm_{0.02,}$ (d) $AgGd_{0.50}(MoO_4)_2:Ho_{0.02}/Yb_{0.45}/Tm_{0.03}$, and (e) $AgGd_{0.45}(MoO_4)_2:Ho_{0.01}/Yb_{0.50}/Tm_{0.04,}$ particles excited by the 514.5-nm line of an Ar ion laser at 0.5 mW.

The ST oxides with the C_{4h} symmetry should show only one spectral band related to the í$_1$ MoO_4 symmetric stretching vibration, but an extra band appears as the right shoulder of the high-intensity peak at 881 cm^{-1}. Such spectral characteristic can be due to the fact that the crystal can have symmetry lower than C_{4h}, for example, S_4 ($I\bar{4}$ space group) [20]. In this case, the crystal structure contains two crystallographically independent MoO_4 tetrahedra and the Raman spectra should be more in line in the range of their vibrations. It is noted that the typical Raman bands were explained in the framework of the local distortions of MoO_4 tetrahedra [28-31]. Consequently, the high efficiency of the $Ho^{3+}/Yb^{3+}/Tm^{3+}$ tri-doped AGM phosphors can be considered as useful white emitting diodes in active optoelectronic devices.

4. Conclusions

The double molybdates of $Ho^{3+}/Yb^{3+}/Tm^{3+}$ tri-doped AGM white phosphors were successfully synthesized by the MES method. All XRD peaks were identified by ST tetragonal cell ($I4_1/a$) with parameters close to $AgEu(MoO_4)_2$ and $NaGd(MoO_4)_2$. The site of (Ag/Eu) or (Na/Gd) ion was occupied by Ag, Gd, Ho, Yb and Tm ions with fixed occupations. The resultant particles samples heated at 850°C for 16 h showed the fine and homogeneous morphology with particle sizes of 3-5 ìm. Under excitation at 980 nm, the doped particles exhibited white emissions corresponding to the $^1G_4$ '! $^3H_6$ transitions of Tm^{3+} in the blue region, the $^5S_2$/ $^5F_4$ '! $^5I_8$ transitions of Ho^{3+} in the green region, the $^5F_5$ '! $^5I_8$ transitions of Ho^{3+} as well as the $^1G_4$ '! $^3F_4$ and $^3H_4$ '! $^3H_6$ transitions of

Tm^{3+} in the red region. For the application for the white emissions, the proper concentration ratio Yb^{3+}:Ho^{3+}+Tm^{3+} was revealed to be 9:1 for white emitting diodes. The calculated chromaticity coordinates were corresponding to the standard equal energy point in CIE diagram. The representative Raman bands were explained in the framework of the local distortions of MoO_4 tetrahedral. It is emphasized that the high efficiency of the $Ho^{3+}/Yb^{3+}/Tm^{3+}$ tri-doped AGM phosphors can be considered as useful white emitting diodes in active optoelectronic devices.

Acknowledgment

This research was supported by the Basic Science Research Program through the National Research Foundation of Korea (NRF) funded by the Ministry of Science, ICT and future Planing (2018R1D1A1A09082321).

References

[1] M.V. DaCosta, S. Doughan, U.J. Krull, Analyca Chimica Acta, 832, 1 (2014).

[2] M. Wang, G. Abbineni, A. Clevenger, C. Mao, S. Xu, Nanomed.: Nanotech. Biol. Med., 7, 710 (2011).

[3] M. Lin, Y. Zho, S. Wang, M, Liu, Z. Duan, Y. Chen, F. Li, F. Xu, T. Lu, Biotechnol. Adv., 30, 1551 (2012).

[4] O. D. Chimitova, V. V. Atuchin, B. G, Bazarov, M. S. Molokeev, Z. G. Bazarova, Proc. SPIE 8771, 877711A (2013).

[5] V.V. Atuchin, O.D. Chimitova, T.A. Gavrilova, M.S. Molokeev, S. J. Kim, N.V. Surovtsev, B.G. Bazarov, , J. Cryst. Growth, 318, 683 (2011).

[6] V.V. Atuchin, O.D. Chimitova, S.V. Adichtchev, J.G. Bazarov, T.A. Gavrilova, M.S. Molokeev, N.V. Surovtsev, Zh.G. Bazarova, , Mater. Lett., 106, 26 (2013).

[7] C.S. Lim, Mater. Res. Bull., 75, 211 (2016).

[8] C.S. Lim, A. Aleksandrovsky, M. Molokeev, A. Oreshonkov, V. Atuchin, Phys. Chem. Chem. Phys., 17, 19278 (2015).

[9] J. Liao, D. Zhou, B. Yang, R. Liu, Q. Zhang, Q. Zhou, J. Lumin., 134, 533-538 (2013).

[10] J. Sun, Y. Lan, Z. Xia, H. Du, Opt. Mater., 33, 576 (2011).

[11] C. Guo, H. K. Yang, J.H. Jeong, J. Lumin., 130, 1390 (2010).

[12] Z. Shan, D. Chen, Y. Yu, P. Huang, F. Weng, H. Lin, Y. Wang, Mater. Res. Bull., 45, 1017 (2010).

[13] W. Liu, J. Sun, X. Li, J. Zhang, Y. Tian, S. Fu, H. Zhong, T. Liu, L. Cheng, H. Xia, B. Dong, R. Hua, X. Zhang, B. Chen, Opt. Mater., 35, 1487 (2013).

[14] W. Xu, H. Zhao, Y. Li, L. Zheng, Z. Zhang, W. Cao, Sensors and Act. B:Chem., 188, 1096 (2013).

[15] C.S. Lim, A. Aleksandrovsky, M. Molokeev, A. Oreshonkov, V. Atuchin, J. Am. Ceram. Soc., 98, 3223 (2015).

[16] C.S. Lim, Mater. Chem. Phys., 131, 714 (2012).

[17] C. S. Lim, A. Aleksandrovsky, M. Molokeev, A. Oreshonkov, D. Ikonnikov, V. Atuchin, Dalton Transactions, 45, 15541 (2016)

[18] C.S. Lim, Mater. Res. Bull., 47, 4220 (2012).

[19] C.S. Lim, Infrar. Phys. Tech., 67, 371 (2014).

[20] C.S.Lim, A. Aleksandrovsky, V. Atuchin, M. Molokeev, A. Oreshonkov, Crystals, 10, 1000-01 (2020).

[21] Bruker AXS TOPAS V4: General profile and structure analysis software for powder diffraction data. – User's Manual. Bruker AXS, Karlsruhe, Germany (2008).

[22] F. Cheng, Z. Xia, M. S. Molokeev, X. Jing, Dalton Transactions, 44, 18078 (2015).

[23] G.M. Kuz'micheva, I.A. Kaurova, E.A. Zagorul'ko, N.B. Bolotina, V.B. Rybakov, A.A. Brykovskiy, E.V. Zharikov, D.A. Lis, K.A. Subbotin, Acta Materialia, 87, 25 (2015).

[24] R. D. Shannon, Acta Cryst., A32, 751 (1976).

[25] F. Anzel, G. Baldacchini, L. Laversenne, G. Boulon, Opt. Mat., 24, 103(2003).

[26] A.A. Savina, V.V. Atuchin, S.F. Solodovnikov, Z.A. Solodovnikova, A.S. Krylov, E.A. Maximovskiy, M.S. Molokeev, A.S. Oreshonkov, A.M. Pugachev, E.G. Khaikina, J. Solid State Chem., 225, 53 (2015).

[27] V.V. Atuchin, V.G. Grossman, S.V. Adichtchev, N.V. Surovtsev, T.A. Gavrilova, B.G. Bazarov, Opt. Mater., 34, 812 (2012).

[28] V.V. Atuchin, O.D. Chimitova, S.V. Adichtchev, J.G. Bazarov, T.A. Gavrilova, M.S. Molokeev, N.V. Surovtsev, Zh.G. Bazarova, Mater. Lett., 106, 26 (2013).

[29] V.V. Atuchin, O.D. Chimitova, T.A. Gavrilova, M.S. Molokeev, Sung-Jin Kim, N.V. Surovtsev, B.G. Bazarov, J. Crys. Growth, 318, 683 (2011).

[30] C.S. Lim, Infrar. Phys. Tech., 76, 353 (2016).

[31] C.S. Lim, A. Aleksandrovsky, M. Molokeev, A. Oreshonkov, V. Atuchin, J. Solid State Chem., 228, 160 (2015).